Comparative Structure and Optical Properties of Ga-, In-, and Sn-Doped ZnO Nanowires Synthesized via Thermal Evaporation

Seung Yong Bae, Chan Woong Na, Ja Hee Kang, and Jeunghee Park*

Department of Chemistry, Korea University, Jochiwon 339-700, South Korea

Received: September 13, 2004; In Final Form: December 1, 2004

ZnO nanowires doped with a high concentration Ga, In, and Sn were synthesized via thermal evaporation. The doping content defined as X/(Zn + X) atomic ratio, where X is the doped element, is about 15% for all nanowires. The nanowires consist of single-crystalline wurtzite ZnO crystal, and the average diameter is 80 nm. The growth direction of vertically aligned Ga-doped nanowires is [001], while that of randomly tilted In- and Sn-doped nanowires is [010]. A correlation between the growth direction and the vertical alignment has been suggested. The broaden X-ray diffraction peaks indicate the lattice distortion caused by the doping, and the broadening is most significant in the case of Sn doping. The absorption and photoluminescence of Sn-doped ZnO nanowires shift to the lower energy region than those of In- and Ga-doped nanowires, probably due to the larger charge density of Sn.

1. Introduction

Zinc oxide (ZnO) is one of the most promising materials for the fabrication of optoelectronic devices operating in the blue and ultraviolet region,[1,2] because of a direct wide band gap (E_g = 3.37 eV at room temperature) and large exciton binding energy (60 meV). Moreover, due to its superior conducting properties based on oxygen vacancies, ZnO has been investigated as transparent conducting and piezoelectric materials for fabricating solar cells, electrodes, and sensors.[3−5] To enhance the electrical/optical properties, ZnO was frequently doped with group III, IV, and V elements (e.g., Al, Ga, In, Sn, and Sb).[6−15] The Al doping increases the conductivity without impairing the optical transmission and is regarded as a potential alternative candidate for indium−tin−oxide (ITO) materials.[6,7] Due to the high reactivity, however, the oxidation of Al source during ZnO growth becomes a problem. The Ga is another excellent dopant in increasing the conductivity, and the source is less reactive and more resistive to oxidation.[8,9] In-doped ZnO films show similar electrical conductivity and better transparency in both the visible and the infrared regions as compared to ITO, so they can be widely used as transparent conductors in many applications.[10,11] It was reported that the Sn-doping increases rather the resistivity of ZnO film and induces an emission at blue wavelength region.[12,13] The grain size and resistivity of ZnO were controlled by the doping levels of Sb.[14,15]

As stimulated by the novel properties of carbon nanotubes, quasi-one-dimensional ZnO nanostructures are currently the subject of intensive research because of the potential for nanoscale electronic and optoelectronic applications.[16−19] The doping of ZnO nanostructures with Ga, In, Sn, Cd, S, Mn, Co, Cu, and Ce elements has become an important issue for the more diverse range of applications, because their electrical, optical, and magnetic properties can be modified.[20−27] In particular, the Ga-doped ZnO nanorods or nanowires were synthesized by a number of research groups.[20] They showed that the Ga doping enhances the conductivity and field emission properties. The Wang group synthesized the In-doped ZnO nanobelts by thermal evaporation.[21] The photoluminescence of those Ga- and In-doped nanostructures becomes broader and shifts to the longer wavelength as compared to the undoped one. The Ren group reported the synthesis of heterostructures that consisted of In- or Sn-doped ZnO nanowire core and ZnO side branches.[22] All works have recently been carried out, and the synthesis and characterization of the doped ZnO nanowires is still a challenging research topic.

Here, we report the syntheses of the ZnO nanowires doped with Ga, In, and Sn, via thermal evaporation at 800−1000 °C. The ultimate goal of the present study is to find the effects of doping on the structure and optical properties of ZnO nanowires. We were able to adjust the doping level by the growth conditions, to compare the structural and optical properties of three different nanowires that are doped with the same content. The content is defined as X/(Zn + X) atomic ratio, where X is the doped element. The ZnO nanowires doped with a high concentration up to 15% and undoped ZnO nanowires were successfully synthesized and thoroughly characterized by scanning electron microscopy (SEM), transmission electron microscopy (TEM), X-ray photoelectron spectroscopy (XPS), high-resolution X-ray diffraction (XRD), UV−visible absorption spectrum, photoluminescence (PL), and cathodoluminescence (CL).

2. Experimental Section

The synthesis was carried using an electrically heated tube furnace. Ga (99.998%, Aldrich), In (99.998%, Aldrich), or Sn (99.998%, Aldrich) powders were placed with ZnO (99.98%, Aldrich) powders in a quartz boat located inside a quartz tube reactor. The Si substrates were coated with $HAuCl_4 \cdot 3H_2O$ (98+%, Sigma) ethanol solution, forming the Au catalytic nanoparticles. The substrate was then placed on the boat containing the source. The flow rate of Ar, the temperature, and the growth time were maintained as 500 sccm, 800−1000 °C, and 2 h, respectively. White-colored film-like product was formed on the whole substrate. For the undoped nanowires, ZnO or Zn (99.998%, Aldrich)/ZnO powder mixture was used, and the substrate was positioned on the quartz boat containing Zn

* Corresponding author. E-mail: parkjh@korea.ac.kr.

10.1021/jp0458708 CCC: $30.25
Published on Web 01/25/2005

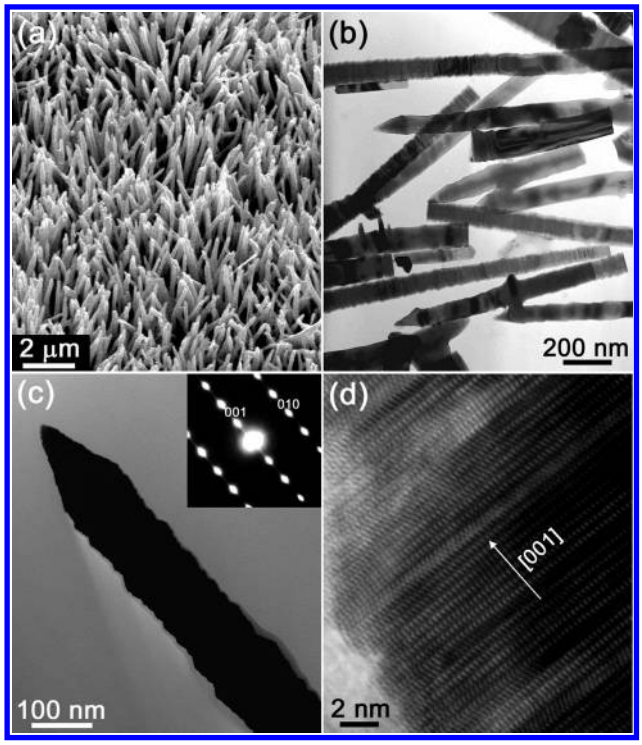

Figure 1. (a) SEM micrograph shows the vertically aligned Ga-doped ZnO nanowires on the substrates. (b) TEM image showing the general morphology of ZnO nanowires. (c) HRTEM image for a typical nanowire with its corresponding SAED pattern (inset). The growth direction is [001]. (d) Atomic-resolved image shows that the distance between neighboring (001) planes is about 5.2 Å.

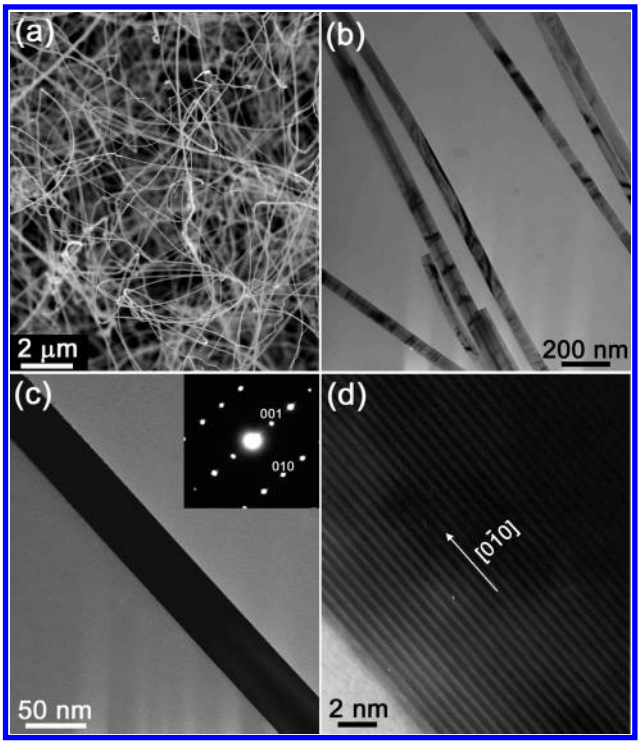

Figure 2. (a) SEM micrograph shows the In-doped ZnO nanowires that randomly tangled on the substrates. (b) TEM image showing the smooth and straight nanowires. (c) HRTEM image for a selected nanowire with its corresponding SAED pattern (inset). (d) Atomic-resolved image shows the (001) planes parallel to the growth direction.

source. The temperature of the reactor was in the range 500−900 °C for 2 h. Argon (Ar) flows with a rate of 500 sccm. Blue tinted white-colored film deposited on the whole substrate. The as-grown materials were characterized and analyzed by SEM (Hitachi S-4300), TEM (JEOL JEM-2010, 200 kV), electron diffraction (ED), and energy-dispersive X-ray spectroscopy (EDX). High-resolution XRD patterns were measured using the 8C2 beam line of the Pohang Light Source (PLS) with monochromatic radiation ($\lambda = 1.5425$ Å). XPS measurement was performed at the 8A1 (Undulator U7) beam line of the PLS. The U7 beam line was designed to provide soft X-rays in the energy range of 50−1500 eV. The XPS data were collected using 1265 eV photon energies, with the photon flux of $\sim 3 \times 10^{10}$ (photons/s/200 mA). The experiment was performed in an ultrahigh vacuum (UHV) chamber with a base pressure $\leq 5 \times 10^{-10}$ Torr. The analyzer was located at 55° from the surface normal. The binding energy was calibrated by using the C 1s peak (284.6 eV). The absorption spectrum has been measured at a reflection mode using a UV−visible spectrophotometer (Cary 2200, Varian Instruments). The PL measurement was carried out at room temperature using a He−Cd laser ($\lambda = 325$ nm) as the excitation source. The laser power was about 1 kW/cm^2. The room-temperature CL (Gatan MonoCL2) measurement was performed at an acceleration voltage of 10 kV.

3. Results and Discussion

Figure 1a corresponds to the SEM image of vertically aligned Ga-doped ZnO nanowires on a large area of the Si substrate. The average length is about 10 μm. The TEM image representing the general morphology of Ga-doped ZnO nanowires is displayed in Figure 1b. The diameter is uniformly 80 nm. The nanowires are straight with a sharp tip, and their surface is slightly rough. Figure 1c shows the high-resolution TEM (HRTEM) image for a typical Ga-doped nanowire. Thin amorphous outerlayers sometimes exist. The selected-area ED (SAED) pattern shows that the nanowire consists of single-crystalline wurtzite ZnO crystal with the [001] growth direction (inset). Figure 1d shows its atomic-resolved image for the edge parts. The (001) fringes perpendicular to the growth direction are separated by 5.2 Å, which is consistent with that of bulk wurtzite ZnO crystal ($a = 3.24982$ Å, $c = 5.20661$ Å; JCPDS Card No. 36-1451). A few stacking faults are found in the lattice planes. All nanowires we observed have the [001] growth direction. EDX identifies that the composition of nanowires is Zn, O, and Ga, as shown in the Supporting Information (Figure S-1). The Cu peak comes from the TEM grid. The Ga content is in the range of 10−25%.

Figures 2a shows the SEM image for high-density In-doped ZnO nanowires that are tangled and frequently form the loops. The nanowires are straight with smooth surface, and the diameter is uniformly 50 nm (Figure 2b). Figure 2c shows the HRTEM image for an In-doped nanowire with its corresponding SAED pattern (inset), revealing a perfect single-crystalline wurtzite ZnO crystal with the [010] growth direction. The (001) fringes parallel to the growth direction are separated by 5.2 Å (Figure 2d). All nanowires have the [010] growth direction. The EDX identifies the composition of individual nanowire to be Zn, O, and In, as shown in the Supporting Information (Figure S-1). The In content is in the range 10−20%.

Figure 3a shows the SEM image for the Sn-doped ZnO nanowires grown homogeneously over a large area of the substrate. The nanowires have the diameter in the range of 40−100 nm (Figure 3b). Figure 3c shows the HRTEM image for a Sn-doped nanowire. The SAED pattern indicates that the nanowire consists of nearly single-crystalline wurtzite ZnO crystal with the [010] growth direction (inset). Figure 3d shows the atomic-resolved image for a selected area of the nanowire.

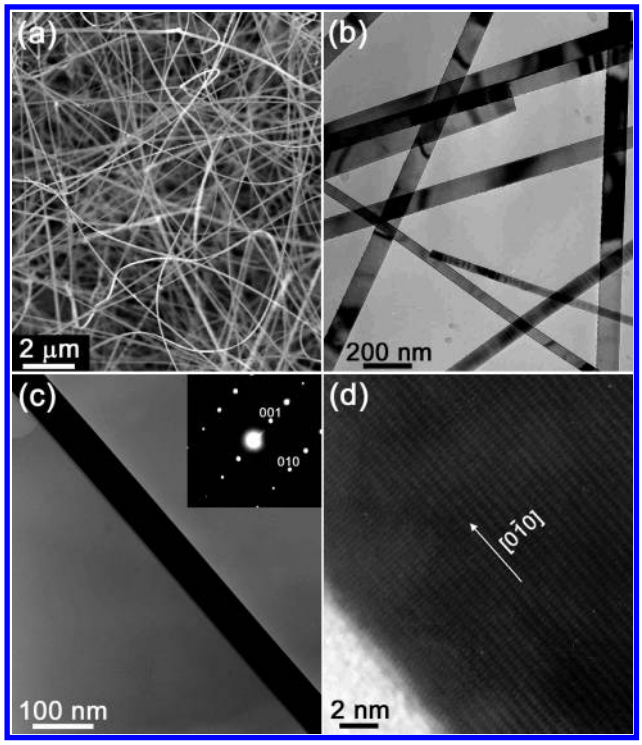

Figure 3. (a) SEM micrograph shows randomly tilted Sn-doped ZnO nanowires. (b) TEM image showing general morphology of nanowires. (c) HRTEM image for a selected nanowire with its corresponding SAED pattern (inset). (d) Atomic-resolved image shows the (001) planes parallel to the growth direction.

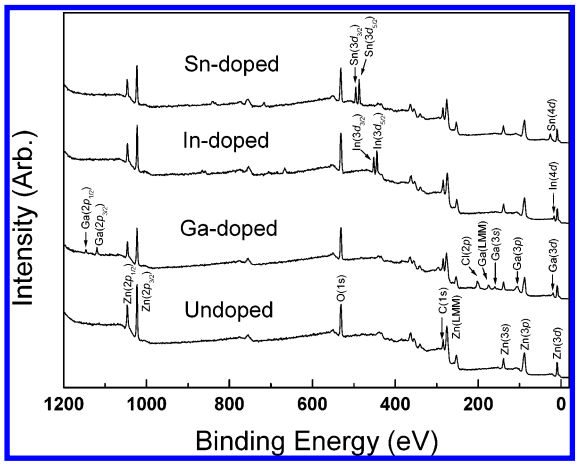

Figure 4. XPS survey scan spectrum of undoped, Ga-, In-, and Sn-doped ZnO nanowires, showing that the content of dopant is about 15%.

The (001) fringes separated by 5.2 Å are parallel to the growth direction. We confirmed that all nanowires have the [010] growth direction. The composition of individual nanowire is identified as Zn, O, and Sn by EDX (Supporting Information Figure S-1). The range of Sn content is 7−20%.

The XPS was used to determine the composition of the doped ZnO nanowires (Figure 4). The undoped ZnO nanowires show Zn and O peaks, with a weak C impurity peak. The peaks located at 1045.6, 1022.6, and 531.6 eV correspond to the electronic state of Zn $2p_{1/2}$, Zn $2p_{3/2}$, and O 1s, respectively. The Ga-doped nanowires show the peaks at 1146.3 and 1119.3 eV, corresponding to the electronic state of Ga $2p_{1/2}$ and Ga $2p_{3/2}$, whose energy gap agrees with the reference value of element, 26.84 eV.[28] The In-doped nanowires show the In $3d_{3/2}$ and In $3d_{5/2}$ peaks located at 451.6 and 444.6 eV, whose gap between two peaks is 7.0 eV that is consistent with the reference value of element, 7.54 eV. The Sn-doped nanowires show the Sn $3d_{3/2}$ and Sn $3d_{5/2}$ peaks located at 494.8 and 486.8 eV, whose gap between two peaks is 8.0 eV that is consistent with the reference value of element, 8.41 eV. Using the atomic sensitivity factors,[28] the average value of Ga, In, and Sn content is estimated to be 15 ± 5%.

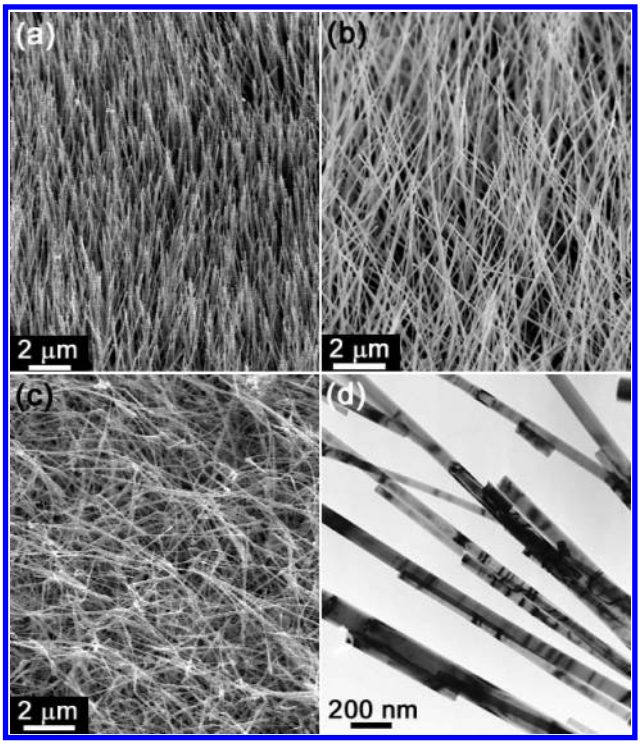

Figure 5. SEM images showing (a) vertically aligned, (b) partially tilted, and (c) all randomly tilted undoped ZnO nanowires. (d) TEM image shows that the average diameter of nanowires is uniformly 80 nm.

The growth of doped ZnO nanowires on the Au nanoparticles-deposited Si substrates would follow a typical vapor−liquid−solid growth mechanism, although the Au nanoparticles were not detected through the TEM analysis. The size of Au nanoparticles is 20−100 nm and defines the diameter of nanowires. The doping content is usually controlled by the growth temperature and relative position of Zn and dopant source to that of the substrates. The Ga-doped nanowires align vertically on the substrates, while the In- and Sn-doped nanowires lie down randomly on the substrates. The growth direction of Ga-doped ZnO nanowires is uniformly [001], but that of In- and Sn-doped nanowires is [010]. The [001] growth direction of vertically aligned Ga-doped nanorods/nanowires and the [010] growth direction of In-doped nanowires/nanobelts were also reported by other research groups.[20−22] So, we could speculate a possible correlation between the vertical alignment and the growth direction. To find it, we synthesized the undoped ZnO nanowires with a controlled alignment and analyzed the growth direction of individual nanowire.

Figure 5a shows the vertically aligned undoped ZnO nanowires synthesized using Zn powders at 500 °C. Figure 5b shows the nanowires synthesized using a Zn/ZnO powder mixture at 800 °C. The vertical alignment is reduced, with a tilted angle of less than 45°. Figure 5c displays the randomly tilted nanowires on the substrates. They were synthesized using a Zn/ZnO powder mixture at 900 °C. As the growth temperature increases to 900 °C, the vertical alignment disappears. The TEM image shows that the nanowires are all straight with smooth

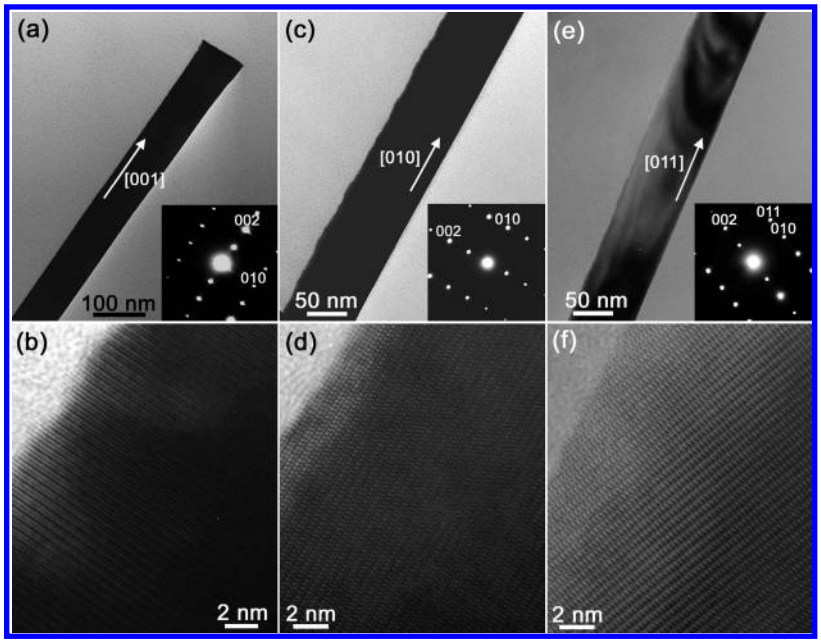

Figure 6. (a) TEM image of a typical undoped ZnO nanowire that is vertically aligned. The SAED pattern reveals the [001] growth direction (inset). (b) Its atomic-resolved image showing the perfect single-crystalline nanowire. (c) TEM image of a typical undoped nanowire whose growth direction is [010], with corresponding SAED (inset). (d) Its atomic-resolved image showing the (001) planes parallel to the growth direction. (e) TEM image for an undoped nanowire whose growth direction is [011], with corresponding SAED (inset). (f) The (001) fringes tilt to the growth direction with an angle of 29°.

surface and their diameter is uniformly 80 nm (Figure 5d). The HRTEM images and SAED pattern reveal that the growth direction of ZnO nanowire is dependent on the vertical alignment. All of the vertically aligned nanowires (Figure 5a) have uniform growth direction [001]. In contrast, the randomly tilted nanowires, as shown in Figure 5c, have preferentially the [010] growth direction, but some of them have other growth directions such as [011]. The partially tilted nanowires (Figure 5b) exhibit mostly the [001] growth direction, but some of them have the [010] growth direction. Therefore, we suggest that the vertically aligned ZnO nanowires would prefer to have the [001] growth direction under our growth conditions. With the enhanced growth rate at the higher temperature, the vertical alignment cannot maintain and the [010] growth direction would be allowed.

Figure 6a shows the HRTEM image of a typical undoped ZnO nanowire that is aligned vertically on the substrates. The SAED pattern reveals a single-crystalline wurtzite ZnO crystal with the [001] growth direction (inset). Figure 6b corresponds to an atomic-resolved image showing the (001) planes perpendicular to the growth direction. Figure 6c shows the HRTEM image of another undoped nanowire whose growth direction is [010]. The SAED pattern reveals a single-crystalline wurtzite ZnO crystal with the [010] growth direction (inset). Figure 6d corresponds to an atomic-resolved image showing the (001) planes parallel to the growth direction. Figure 6e corresponds to the nanowire grown with the [011] growth direction. The SAED confirms the [011] growth direction (inset). The (001) fringes skew to the growth direction by an angle of 29° (Figure 6f).

For the growth of In- and Sn-doped ZnO nanowires, the temperature range of 900−1000 °C was used. At the temperatures above 1000 °C, the formation of In_2O_3, SnO_2, and spinel-typed Zn_2SnO_4 alloy nanowires takes place. The doping content of In and Sn was negligible at the temperatures lower than 900 °C. In contrast, we inevitably used the lower temperature range 800−900 °C for the Ga doping, to avoid the growth of Ga_2O_3

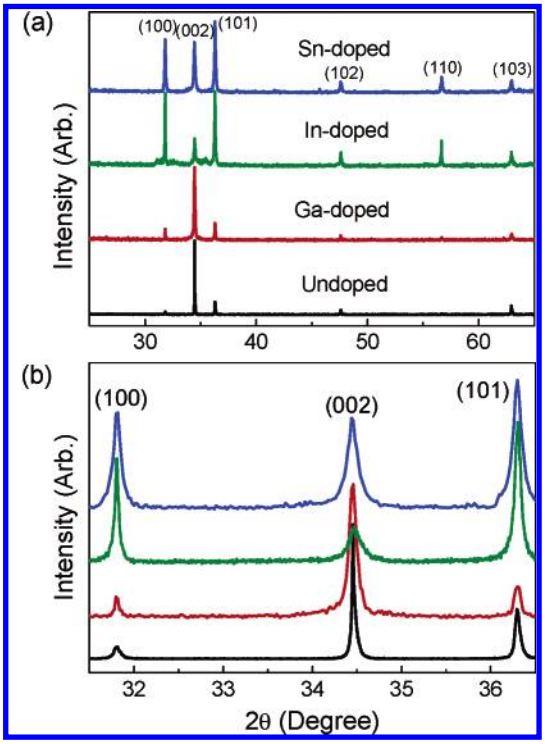

Figure 7. (a) Full-range XRD pattern taken from the undoped, Ga-, In-, and Sn-doped ZnO nanowires. (b) The fine-scanned (100), (002), and (101) peaks, showing the peak broadening due to the doping.

nanowires at the temperatures higher than 900 °C. Thus, the [010] growth direction of randomly tilted In- and Sn-doped ZnO nanowires possibly results from the faster growth rates at the higher growth temperature. The [001] growth direction of Ga-doped nanowires would be linked with their vertical alignment at the lower growth temperature. The larger diameter of Ga-doped ZnO nanowires than that of In- and Sn-doped nanowires may be related to the slower growth rate at the lower temperature.

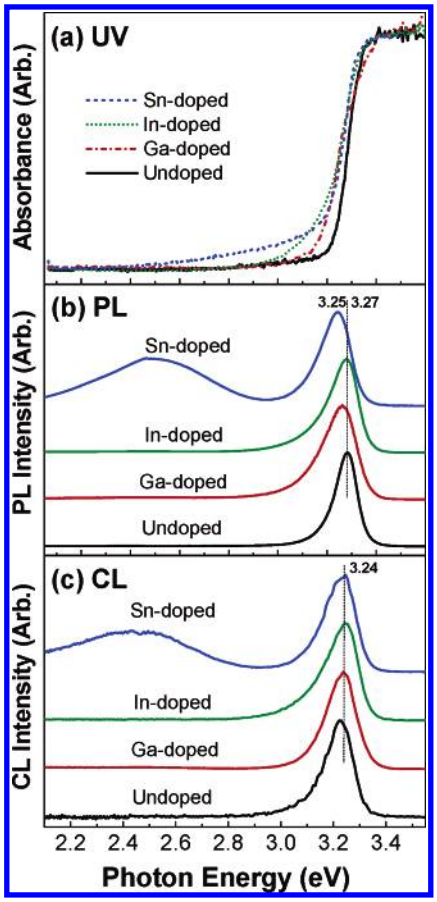

Figure 8. (a) UV−visible absorption, (b) PL, and (c) CL spectrum of undoped and doped ZnO nanowires measured at room temperature. The excitation wavelength of PL is the 325 nm line of a He−Cd laser, and the acceleration voltage of CL is 10 kV.

The high-resolution XRD pattern was measured for undoped, Ga-, In-, and Sn-doped ZnO nanowires. The undoped nanowires were grown at 800 °C, as shown in Figure 5b. Figure 7a displays the full-range XRD patterns, showing the major peaks of wurtzite ZnO crystals. For the undoped and Ga-doped nanowires, the strongest peak is (002), which is due to the vertical alignment and the [001] growth direction. The (100), (002), and (101) peaks in the range $2\theta = 31-37°$ are displayed in Figure 7b. The peak width of doped nanowires is much broader than that of undoped nanowires, indicating a lattice distortion due to the introduction of other elements. It is noticed that the most significant broadening takes place in the Sn-doped nanowires. The radius of Zn and doped elements in the wurtzite ZnO crystal is expected to be $r(Zn^{2+}) = 74$ pm, $r(Ga^{3+}) = 61$ pm, $r(In^{3+}) = 76$ pm, and $r(Sn^{4+}) = 69$ pm.[29] The respective charge is +2, +3, +3, and +4. Therefore, the largest charge density of Sn would deform the ZnO lattices more significantly than the others. The peak positions are about the same for the undoped, Ga-, and Sn-doped nanowires. The In-doped nanowires exhibit a slightly lower angle shift of (100) and (101) peaks from that of undoped nanowires by 0.02°, which is possibly related to the larger radius than Zn.

As the ZnO nanowires are doped, the absorbance curve of the UV−visible absorption spectrum becomes broader with a lower energy shift (Figure 8a). It gives a direct evidence for the decrease of band gap (E_g) and the energy broadening of valence band states attributable to the doping. As the doped elements enter the ZnO crystal lattices, the localized band edge states form at the doped sites, with a reduction of E_g. The broadening down to the lower energy region takes place most considerably for the Sn doping.

Figures 8b displays the PL spectrum of four ZnO nanowire samples measured at room temperature. The excitation energy is 3.815 eV. The undoped ZnO nanowires exhibit the peak at 3.27 eV corresponding to the near band edge (NBE) peak that is responsible for the recombination of free excitons of ZnO.[30,31] The doped ZnO nanowires all show the broad NBE peak at the lower energy region, providing another evidence for the E_g decrease. The full-width at half-maximum increases by a factor of 1.5. The peak position of the Sn-doped nanowires shifts to the lower energy 3.25 eV. In particular, the Sn-doped nanowires have a green emission band around 2.5 eV that originates from the recombination of the holes with the electrons occupying the singly ionized O vacancies.[32] The largest charge density of Sn will give rise to more defects such as oxygen vacancies, which result in the great enhancement of green emission. Figure 8c displays the CL spectrum of four ZnO nanowire samples measured at room temperature. It shows the NBE peak at around 3.24 eV, the broader width caused by the doping, and the enhanced green emission for the Sn doping, which are all consistent with the results of PL. From the result of XRD pattern and absorption/emission spectra, we suggest that the band gap as well as the optical properties of ZnO nanowires can be controlled by selecting the doping element.

4. Conclusions

We synthesized high-density undoped, Ga-, In-, and Sn-doped ZnO nanowires on the Au nanoparticles-deposited Si substrates via thermal evaporation at 500−1000 °C. The average diameter of ZnO nanowires is 80 nm. The HRTEM images and SAED patterns confirm that all ZnO nanowires consist of single-crystalline wurtzite ZnO crystal. The EDX and XPS data reveal that the average content is as high as about 15% for all three dopants. The vertically aligned Ga-doped ZnO nanowires were grown with the [001] direction. In contrast, the growth direction of randomly tilted In- and Sn-doped ZnO nanowires is [010]. We discuss a correlation between the growth direction and the vertical alignment, using the undoped ZnO nanowires grown with the controlled vertical alignment.

The broadened XRD peaks of the doped ZnO nanowires indicate the lattice distortion attributable to the doping. The UV−visible absorption spectrum reveals the E_g decrease that would be originated from the localized band edge states at the doping sites. The PL and CL of the doped ZnO nanowires show a broader NBE band at the lower energy range as compared to that of undoped ZnO nanowires, due to the E_g decrease at the doping sites. The Sn doping causes the largest XRD peak broadening, most significant E_g reduction, and strong green emission, which would be due to the largest charge density of Sn. It suggests that the charge density of doped element would be an important parameter in controlling the optical properties of ZnO nanowires.

Acknowledgment. This work was supported by KOSEF (Project No.: R14-2004-033-01003-0, R02-2004-000-10025) and KRF (Project No.: 2004-015-C00265). SEM and XRD analysis was performed at Korea Basic Science Institute in Seoul. Experiments at PLS were supported in part by MOST and POSTECH.

Supporting Information Available: Figure showing the EDX spectra of Ga-, In-, and Sn-doped nanowires. This material is available free of charge via the Internet at http://pubs.acs.org.

References and Notes

(1) Cao, H.; Xu, J. Y.; Zhang, D. Z.; Chang, S.-H.; Ho, S. T.; Seelig, E. W.; Liu, X.; Chang, R. P. H. *Phys. Rev. Lett.* **2000**, *84*, 5584.

(2) Saito, N.; Haneda, H.; Sekiguchi, T.; Ohashi, N.; Sakaguchi, I.; Koumoto, K. *Adv. Mater.* **2002**, *14*, 418.

(3) Contreras, M. A.; Egaas, B.; Ramanathan, K.; Hiltner, J.; Swartzlander, A.; Hasoon, F.; Noufi, R. *Prog. Photovoltaics* **1999**, *7*, 311.

(4) Rau, U.; Schmidt, N. *Thin Solid Films* **2001**, *387*, 141.

(5) Dong, L. F.; Cui, Z. L.; Zhang, Z. K. *Nanostruct. Mater.* **1997**, *8*, 815.

(6) Cebulla, R.; Wendt, R.; Ellmer, K. *J. Appl. Phys.* **1998**, *83*, 1087.

(7) Ma, J.; Ji, F.; Zhang, D.-H.; Ma, H.-L.; Li, S.-Y. *Thin Solid Films* **1999**, *357*, 98.

(8) Hu, J.; Gordon, R. G. *J. Appl. Phys.* **1992**, *72*, 5381.

(9) Wang, R.; Sleight, A. W.; Cleary, D. *Chem. Mater.* **1996**, *8*, 433.

(10) Gómez, H.; Maldonado, A.; Asomoza, R.; Zironi, E. P.; Cañetas-Ortega, J.; Palacios-Gómez, J. *Thin Solid Films* **1997**, *293*, 117.

(11) Wang, A.; Dai, J.; Cheng, J.; Chudzik, M. P.; Marks, T. J.; Chang, R. P. H.; Kannewurf, C. R. *Appl. Phys. Lett.* **1998**, *73*, 327.

(12) Sato, H.; Minami, T.; Takata, S. *J. Vac. Sci. Technol., A* **1993**, *11*, 2975.

(13) Bougrine, A.; El Hichou, A.; Addou, M.; Ebothé, J.; Kachouane, A.; Troyon, M. *Mater. Chem. Phys.* **2003**, *80*, 438.

(14) Dayan, N. J.; Karekar, R. N.; Aiyer, R. C.; Sainkar, S. R. *J. Mater. Sci.: Mater. Electron.* **1997**, *8*, 277.

(15) Gulino, A.; Fragala, I. *Chem. Mater.* **2002**, *14*, 116.

(16) (a) Huang, M. H.; Mao, S.; Feick, H.; Yan, H.; Wu, Y.; Kind, H.; Weber, E.; Russo, R.; Yang, P. *Science* **2001**, *292*, 1897. (b) Park, W. I.; Yi, G.-C.; Kim, M.; Pennycook, S. J. *Adv. Mater.* **2003**, *15*, 526. (c) Choy, J.-H.; Jang, E.-S.; Won, J.-H.; Chung, J.-H.; Jang, D.-J.; Kim, Y.-W. *Adv. Mater.* **2003**, *15*, 1911.

(17) (a) Lee, C. J.; Lee, T. J.; Lyu, S. C.; Zhang, Y.; Ruh, H.; Lee, H. J. *Appl. Phys. Lett.* **2002**, *81*, 3648. (b) Wan, Q.; Yu, K.; Wang, T. H.; Lin, C. L. *Appl. Phys. Lett.* **2003**, *83*, 2253. (c) Xu, C. X.; Sun, X. W. *Appl. Phys. Lett.* **2003**, *83*, 380. (d) Li, Y. B.; Bando, Y.; Goldberg, D. *Appl. Phys. Lett.* **2004**, *84*, 3603. (e) Li, Q. H.; Wan, Q.; Chen, Y. J.; Wang, T. H.; Jia, H. B.; Yu, D. P. *Appl. Phys. Lett.* **2004**, *84*, 636.

(18) (a) Arnold, M. S.; Avouris, P.; Pan, Z. L.; Wang, Z. L. *J. Phys. Chem. B* **2003**, *107*, 659. (b) Wan, Q.; Li, Q. H.; Chen, Y. J.; Wang, T. H.; He, X. L.; Li, J. P.; Lin, C. L. *Appl. Phys. Lett.* **2004**, *84*, 3654. (c) Ng, H. T.; Han, J.; Yamada, T.; Nguyen, P.; Chen, Y. P.; Meyyappan, M. *Nano Lett.* **2004**, *4*, 1247.

(19) (a) Kind, H.; Yan, H.; Messer, B.; Matthew, L.; Yang, P. *Adv. Mater.* **2002**, *14*, 158. (b) Keem, K. I.; Kim, H.; Kim, G.-T.; Lee, J. S.; Min, B.; Cho, K.; Sung, M.-Y.; Kim, S. *Appl. Phys. Lett.* **2004**, *84*, 4376. (c) Li, Q. H.; Wan, Q.; Liang, Y. X.; Wang, T. H. *Appl. Phys. Lett.* **2004**, *84*, 4556. (d) Ahn, S. E.; Lee, J. S.; Kim, H.; Kim, S.; Kang, B. H.; Kim, K. H.; Kim, G. T. *Appl. Phys. Lett.* **2004**, *84*, 5022.

(20) (a) Tseng, Y.-K.; Huang, C.-J.; Cheng, H.-M.; Lin, I.-N.; Liu, K.-S.; Chen, I.-C. *Adv. Funct. Mater.* **2003**, *13*, 811. (b) Yan, M.; Zhang, H. T.; Widjaja, E. J.; Chang, R. P. H. *J. Appl. Phys.* **2003**, *94*, 5240. (c) Zhong, J.; Muthukumar, S.; Chen, Y.; Lu, Y.; Ng, H. M.; Jiang, W.; Garfunkel, E. L. *Appl. Phys. Lett.* **2003**, *83*, 3401. (d) Xu, C. X.; Sun, X. W.; Chen, B. J.; Shum, P.; Li, S.; Hu, X. *J. Appl. Phys.* **2004**, *95*, 661. (e) Xu, C. X.; Sun, X. W.; Chen, B. J. *Appl. Phys. Lett.* **2004**, *84*, 1540.

(21) Jie, J.; Wang, G.; Han, X.; Yu, Q.; Liao, Y.; Li, G.; Hou, J. G. *Chem. Phys. Lett.* **2004**, *387*, 466.

(22) Wen, J. G.; Lao, J. Y.; Wang, D. Z.; Kyaw, T. M.; Foo, Y. L.; Ren, Z. F. *Chem. Phys. Lett.* **2003**, *372*, 717.

(23) Wan, Q.; Li, H.; Chen, Y. J.; Wang, T. H.; He, X. L.; Gao, X. G.; Li, J. P. *Appl. Phys. Lett.* **2004**, *84*, 3085.

(24) (a) Geng, B. Y.; Wang, G. Z.; Jiang, Z.; Xie, T.; Sun, S. H.; Meng, G. W.; Zhang, L. D. *Appl. Phys. Lett.* **2003**, *82*, 4791. (b) Bae, S. Y.; Seo, H. W.; Park, J. *J. Phys. Chem. B* **2004**, *108*, 5206.

(25) (a) Ip, K.; Frazier, R. L.; Heo, Y. W.; Norton, D. P.; Abernathy, C. R.; Pearton, S. J.; Kelly, J.; Rairigh, R.; Hebard, A. F.; Zavada, J. M.; Wilson, R. G. *J. Vac. Sci. Technol., B* **2003**, *21*, 1476. (b) Chang, Y. Q.; Wang, D. B.; Luo, X. H.; Xu, X. Y.; Chen, X. H.; Li, L.; Chen, C. P.; Wang, R. M.; Xu, J.; Yu, D. P. *Appl. Phys. Lett.* **2003**, *83*, 4020. (c) Ronning, C.; Gao, P. X.; Ding, Y.; Wang, Z. L. *Appl. Phys. Lett.* **2004**, *84*, 784.

(26) Xu, C. X.; Sun, X. W.; Zhang, X. H.; Ke, L.; Chua, S. J. *Nanotechnology* **2004**, *15*, 856.

(27) Cheng, B.; Xiao, Y.; Wu, G.; Zhang, L. *Appl. Phys. Lett.* **2004**, *84*, 416.

(28) Moulder, J. F.; Sticks, W. F.; Sobol, P. E.; Bomben, K. D. *Handbook of X-ray Photoelectron Spectroscopy*; Physical Electronics Inc.: USA, 1995.

(29) Shannon, R. D. *Acta Crystallogr.* **1976**, *A32*, 751.

(30) Kong, Y. C.; Yu, D. P.; Zhang, B.; Fang, W.; Feng, S. Q. *Appl. Phys. Lett.* **2001**, *78*, 407.

(31) Park, W. I.; Jun, Y. H.; Jung, S. W.; Yi, G.-C. *Appl. Phys. Lett.* **2003**, *82*, 964.

(32) Vanheusden, K.; Warren, W. L.; Seager, C. H.; Tallant, D. R.; Voigt, J. A.; Gnade, B. E. *J. Appl. Phys.* **1996**, *79*, 7983.